Published in final edited form as:

Biomaterials. 2016 June ; 92: 1–12. doi:10.1016/j.biomaterials.2016.03.024.

In vivo xenogeneic scaffold fate is determined by residual antigenicity and extracellular matrix preservation

Maelene L. Wong[a,b], **Janelle L. Wong**[a], **Natalia Vapniarsky**[b], and **Leigh G. Griffiths**[a,*]

[a]Department of Veterinary Medicine and Epidemiology, University of California, Davis, One Shields Ave., Davis, CA 95616, USA

[b]Department of Biomedical Engineering, University of California, Davis, One Shields Ave., Davis, CA 95616, USA

Abstract

The immunological potential of animal-derived tissues and organs is the critical hurdle to increasing their clinical implementation. Glutaraldehyde-fixation cross-links proteins in xenogeneic tissues (e.g., bovine pericardium) to delay immune rejection, but also compromises the regenerative potential of the resultant biomaterial. Unfixed xenogeneic biomaterials in which xenoantigenicity has been ameliorated and native extracellular matrix (ECM) architecture has been maintained have the potential to overcome limitations of current clinically utilized glutaraldehyde-fixed biomaterials. The objective of this work was to determine how residual antigenicity and ECM architecture preservation modulate recipient immune and regenerative responses towards unfixed bovine pericardium (BP) ECM scaffolds. Disruption of ECM architecture during scaffold generation, with either SDS-decellularization or glutaraldehyde-fixation, stimulated recipient foreign body response and resultant fibrotic encapsulation following leporine subpannicular implantation. Conversely, BP scaffolds subjected to stepwise removal of hydrophilic and lipophilic antigens using amidosulfobetaine-14 (ASB-14) maintained native ECM architecture and thereby avoided fibrotic encapsulation. Removal of hydrophilic and lipophilic antigens significantly decreased local and systemic graft-specific, adaptive immune responses and subsequent calcification of BP scaffolds compared to scaffolds undergoing hydrophile removal only. Critically, removal of antigenic components and preservation of ECM architecture with ASB-14 promoted full-thickness recipient non-immune cellular repopulation of the BP scaffold. Further, unlike clinically utilized fixed BP, ASB-14-treated scaffolds fostered rapid intimal and medial vessel wall regeneration in a porcine carotid patch angioplasty model. This work highlights the importance of residual antigenicity and ECM architecture preservation in modulating recipient immune and regenerative responses towards xenogeneic biomaterial generation.

*Corresponding author. lggriffiths@ucdavis.edu (L.G. Griffiths).

Disclosures

Drs. Griffiths and Wong are ViVita Technologies, Inc. co-founders and shareholders. Dr. Griffiths serves as Chairman and Dr. Wong serves as CEO and CTO. Porcine work was performed under U.S. Air Force Surgeon General-approved Clinical Investigation No. FDG20140011A. The expressed views are those of the authors and do not reflect the official policy or position of the U.S. Government, Department of Defense, or Department of the Air Force.

Keywords

Antigen removal; Decellularization; Xenogeneic scaffold; Extracellular matrix; Vascular regenerative medicine; Immune response

1. Introduction

Xenogeneic tissues have found clinical utility as surgical patches in various sites of the body. For instance, towards vascular repair, glutaraldehyde-fixed bovine pericardium (BP) patches are advantageous due to ready availability, decreased suture line bleeding, durability, and strength [1,2]. Further, ability for immediate insonation and reduced restenosis risk motivates use of BP over synthetic patches [2]. Unfortunately, current glutaraldehyde-fixation processes employed to increase BP immune-compatibility for clinical applications limit recipient cellular ingrowth and subsequent extracellular matrix (ECM) remodeling in response to the dynamic physiological environment [3–5]. With limited ability to adaptively remodel [5], these non-viable biomaterials are associated with risk for either aneurysmal dilation or stenosis [1]. By avoiding fixation, ECM-based biomaterials derived from xenogeneic tissues may retain capacity for cellular repopulation and regenerative processes.

Xenoantigenicity represents the major barrier to immune-compatibility (i.e., avoidance of destructive, recipient, graft-specific immune responses) and expanded use of unfixed xenogeneic biomaterials in clinical practice. Galactose-α(1,3)-galactose (α-gal) and major histocompatibility complex class I (MHC I) are two xenoantigens known to elicit immune rejection upon implantation [6,7]. The carbohydrate moiety α-gal is ubiquitous in non-primate mammals and New World Monkeys; absence of α-gal in humans and Old World Monkeys results in constitutive production of the corresponding xenoreactive anti-Gal antibody [8,9]. Consequently, α-gal is the primary mediator of hyperacute rejection in discordant xenotransplantation [7]. Present on the surface of all nucleated cells, MHC I molecules elicit both innate and adaptive xenogeneic immune responses [6,7]. Recognition and presentation of non-self, major or minor histocompatibility antigens to T-cells activates the adaptive immune response [10]. Resultant cytokine secretion promotes recruitment and activation of additional innate and adaptive immune cells for graft-specific, cell-mediated immune rejection [7]. Concurrently, recognition and presentation of non-self antigens to helper T-cells by B-cells initiates B-cell maturation, isotype switching, and antibody secretion [10]. Local lymphoid follicle formation creates a site for new graft-specific lymphocyte development. These immunological challenges motivate efforts to achieve xenoantigen removal from tissues and organs, to yield intact ECM to serve as a scaffold for tissue engineering and regenerative medicine applications. Non-fixation approaches to reduce ECM scaffold xenoantigenicity include decellularization [11,12], targeted removal of known antigens [13–16], and physiochemical property-based removal of unknown antigens [17,18]. Stepwise, solubilization-based removal of xenoantigens from BP, using dithiothreitol and KCl for hydrophiles, followed by amidosulfobetaine-14 (ASB-14) for lipophiles, significantly reduces residual hydrophilic [17] and lipophilic [18] antigens, including detectable α-gal and MHC I in the resultant scaffold. However, the extent to which

persistent hydrophilic and lipophilic antigens in xenogeneic scaffolds modulate recipient adaptive immune responses *in vivo* is currently unknown.

Maintenance of native ECM architecture to promote recipient recognition of the scaffolds as self in origin represents a second critical hurdle to generation of regenerative xenogeneic biomaterials. Fibrous encapsulation of synthetic implants is attributed to innate cells being unable to recognize the implant as self [19,20]. Cells of the innate immune system perpetually survey tissues for foreign substances and have been linked to cell-mediated xenograft rejection [7]. Persistence of foreign (i.e., non-self) material stimulates a foreign body response, characterized by giant cell formation and graft fibrous encapsulation [19]. Following isolation from the rest of the body by formation of a fibrous capsule [21], the graft is rendered non-viable [22] and subsequently unable to undergo regenerative processes. Through preservation of native ECM architecture (e.g., morphology, collagen alignment, and thermal stability), it is possible that innate cells probing the xenogeneic scaffold may identify the implant as self. In turn, foreign body response and subsequent fibrous encapsulation of the graft may be avoided. However, the degree to which alterations in ECM architecture of xenogeneic scaffolds affect *in vivo* innate and regenerative responses has not been previously been investigated.

In this study, we determined the ability of various levels of residual antigenicity and ECM preservation to modulate beneficial and deleterious *in vivo* adaptive, innate, and regenerative responses towards BP-based biomaterials.

2. Materials and methods

Detailed Materials and Methods can be found as Supplementary Information. All chemicals were purchased from Sigma-Aldrich unless otherwise stated.

2.1. Tissue harvest

Frozen bovine pericardium from adult cattle (Spear Products) was thawed and placed into PBS (pH 7.4) with 0.1% (w/v) EDTA and 1% (v/v) Antibiotic Antimycotic Solution (AAS). Pericardial fat and loose connective tissue was removed. Circumferentially trimmed strips were stored in Dulbecco's Modified Eagles Medium (DMEM) containing 15% (v/v) dimethyl sulfoxide (DMSO) at −80 °C.

2.2. Sample preparation

BP was subjected to antigen removal 4 °C and 125 rpm unless otherwise stated, as previously described [17,18]. For *in vitro* characterization and rabbit implantation, sets of four anatomically-adjacent BP pieces (1.0 cm × 1.5 cm) were generated: one piece for native control and one for each of three treatments (Table 1): (i) hydrophilic antigen removal using optimized solubilizing antigen removal buffer (opt SARB; 10 mM Tris-HCl, pH 8.0 with 100 mM dithiothreitol, 100 mM KCl, 2 mM $MgCl_2$–$6H_2O$, 0.5 mM Pefabloc SC (Roche), 1% (v/v) AAS) only for 96 h; (ii) hydrophilic antigen removal using opt SARB for 48 h, followed by lipophilic antigen removal using 1% (w/v) ASB-14 in opt SARB at room temperature for 48 h; or (iii) decellularization using 0.1% (w/v) SDS (Bio-Rad) in basic antigen removal buffer (BARB; 10 mM Tris-HCl, pH 8.0 with 0.5 mM Pefabloc SC, 1%

(v/v) AAS) for 48 h, followed by 1% (w/v) SDS in BARB at room temperature for 48 h. Antigen removed or decellularized BP then underwent nucleic acid digestion (10 mM Tris-HCl, pH 7.6 with 2.5 Kunitz units/mL DNase I, 7.5 Kunitz units/mL RNase A, 0.15 M NaCl, 2 mM $MgCl_2$–$6H_2O$, and 1% (v/v) AAS in) for 24 h, and washout (20 mM Tris-buffered saline, pH 7.5 with 0.5 mM Pefabloc SC and 1% (v/v) AAS) for 48 h. For pig implantation, BP pieces (2.0 cm × 1.5 cm) were subjected to antigen removal using either opt SARB only or opt SARB, followed by ASB-14.

2.3. Western blot

One-dimensional electrophoresis and Western blot was performed using equal volumes of residual hydrophilic or lipophilic BP protein extract (n = 6 per group), as previously described [17,18]. To assess persistence of known xenoantigens, blots were probed with either anti-Galα1-3Galβ1-(3)4GlcNAc-R) (M86; Enzo Life Sciences) or anti-bovine MHC I (IL-A88; Bio-Rad AbD Serotec).

2.4. Scanning electron microscopy

Two 5 mm diameter discs from each scaffold (n = 3 per group) were mounted with opposite sides facing up and analyzed on a scanning electron microscope (Philips XL30 TMP; FEI Company).

2.5. Differential scanning calorimetry

ECM thermal stability was determined using an adaptation of a method previously described [23]. Briefly, 5 mm diameter discs (punched from an initial 0.2 g piece, n = 6 per group) were lyophilized (0.8–5.7 mg in dry weight), crimped in aluminum pans, and heated (30–280 °C at 20 °C/min and 10 min hold at 120 °C) using a differential scanning calorimeter (DSC 6000; Perkin Elmer, Waltham, MA). Denaturation temperature was determined with Pyris software (version 11.1.1.0497, Perkin Elmer).

2.6. Leporine subpannicular implantation

The rabbit study was conducted under approval from the University of California, Davis IACUC. A subpannicular pocket was created in forty skeletally mature, female New Zealand White rabbits (n = 8 per group). A 1.0 × 1.5 cm BP implant (native BP, opt SARB scaffold, ASB-14 scaffold, SDS scaffold, or glutaraldehyde-fixed BP (St. Jude Medical) was placed into the pocket and skin routinely closed. Rabbit blood and serum were collected pre-implantation (0 d) and post-implantation (7, 14, 28, 42 d). Following euthanasia at 7 d (n = 2 per group) and 42 d (n = 6 per group), implanted BP and surrounding tissue was excised en bloc.

2.7. Porcine patch angioplasty

The rabbit study was conducted under approval from the Travis Air Force Base 60th Medical Group IACUC. A longitudinal arteriotomy was created in the right carotid artery of nine skeletally mature Yorkshire farm pigs (n = 3 per group). A 2.0 × 0.5 cm elliptical-shaped vessel patch (opt SARB scaffold, ASB-14 scaffold, or glutaraldehyde-fixed BP) was

sutured into the arteriotomy incision. Following euthanasia at 28 d post-implantation, right carotid artery was excised en bloc.

2.8. Porcine ultrasound and angiography

Duplex and B-mode ultrasound examination of patched arteries (at 28 d) was used to assess for presence of stenosis, aneurysm, or turbulence (Acuson X300 with VF8-3 transducer; Siemens). Pulsed-wave Doppler was used to assess maximal blood flow velocity. Right carotid angiography (at 28 d) was used to assess normal and patched regions of the right carotid artery for presence of stenosis or aneurysm (OEC 9900 Elite; GE Healthcare with 5 Fr catheter; Arrow International).

2.9. Elisa

Homogenized native BP was immobilized and probed with rabbit sera (0, 7, 14, 28, and 42 d post-implantation, $n = 6$ per group). Linear regression of the reference curve was used to extrapolate fold-change of graft-specific antibodies over time. Antibody titers at 7, 14, 28, and 42 d were normalized to 0 d for each rabbit, allowing expression of all data as fold-increase over baseline.

2.10. Histology

Picrosirius red-stained scaffold sections were assessed for collagen alignment under polarized light. Collagen alignment was quantified as percent area of collagen birefringence from high-powered fields (HPFs) taken randomly throughout implants ($n = 3$ HPFs per sample, $n = 6$ per group).

Hematoxylin and eosin (H&E)-stained rabbit explant sections (42 d) were independently scored by two blinded observers using a board-certified veterinary pathologist-developed grading scheme to rank severity of recipient response (Table 2). Fibrous capsule thickness was quantified using ImageJ (NIH) from HPFs taken randomly around the implant periphery ($n = 3$ measurements per HPF; $n = 4$ HPFs per sample; $n = 6$ per group). Picrosirius red-stained explant sections (42 d) were assessed for collagen alignment as described above. Von Kossa-stained explant sections (42 d) were assessed for degree of scaffold calcification using NIS Elements (Nikon). To account for heterogeneity of calcium deposits throughout the implant, the lowest magnification at which calcification was observed was determined. At representative sites of calcification, area of individual calcium deposits was quantified and percent area of calcification per HPF was calculated ($n = 3$ HPFs per sample, $n = 6$ per group).

H&E-stained porcine explant sections (28 d) were assessed by a board-certified veterinary pathologist for recipient response to BP patch. Neointimal and neomedial wall thickness middle and end of patch was normalized to tunica media of proximal native carotid artery ($n = 3$ measurements per HPF; $n = 3$ per group).

2.11. Immunohistochemistry

Rabbit explants (42 d) were stained for macrophage (MAC387; Abcam) and T-cell (CD3; courtesy of Dr. Peter Moore) presence throughout the scaffold and adjacent tissue. Pig

explants (28 d) were stained for T-cell (CD3, SP7; Abcam), B-cell (CD79a, HM47/A9; Abcam), M1 macrophage (CCR7, C-terminal; Abcam), M2 macrophage (CD163; Abcam), endothelial cell (CD31; Abcam), and smooth muscle cell (αSMA, 1A4; Abcam) presence throughout the scaffold and adjacent tissue. Ratio of M2 to M1 macrophages was quantified from HPFs using NIS Elements at the implant middle and end ($n = 2$ HPFs per sample, $n = 3$ per group) to determine whether the implant was pro-inflammatory (M1 > M2) or pro-regenerative (M1 < M2).

2.12. Statistical analysis

Non-repeated measures ANOVA and Tukey-Kramer HSD *post hoc* analyses were performed on sample means. Repeated measures ANOVA and Tukey HSD *post hoc* analysis was performed on least squares means. Wilcoxon/Kruskal-Wallis Test and Wilcoxon Method *post hoc* analysis was performed on non-parametric medians. All data are presented as mean ± standard deviation unless otherwise stated using statistical significance of $p < 0.05$.

3. Results

3.1. Removal of hydrophilic and lipophilic antigens reduces recipient adaptive immune response

To understand the effect of residual antigenicity on recipient adaptive immune responses, BP scaffolds (Table 1) were characterized for persistence of known xenoantigens MHC I and α-gal. Following 42 d leporine subpannicular implantation, systemic (i.e., temporal graft-specific IgG titers) and local (i.e., peri-implant T-cells and lymphoid follicles) adaptive immune responses to BP scaffolds were assessed. Hydrophile solubilization using dithiothreitol and KCl (i.e., opt SARB) has been demonstrated to reduce residual hydrophobic antigenicity of BP by 80% compared to decellularization using hypotonic solution and 60% compared to decellularization using SDS [17]. A second step of lipophile solubilization using ASB-14 reduced residual lipophilic antigenicity of BP by 60% compared to hypotonic solution [18]. Furthermore, this stepwise, solubilization-based antigen removal approach was reported to eliminate immunohistochemical detection of α-gal and MHC I in the resultant scaffold [18]. Here, stepwise, solubilization-based removal of hydrophilic antigens using opt SARB, followed by removal of lipophilic antigens using ASB-14 significantly reduced known xenoantigens MHC I ($1.20 \times 10^5 \pm 5.69 \times 10^4$ integrated density value (IDV)) and α-gal ($4.66 \times 10^6 \pm 6.19 \times 10^6$ IDV) from levels present in both native BP ($5.24 \times 10^5 \pm 2.34 \times 10^5$ IDV, $p = 0.0001$ and $4.29 \times 10^7 \pm 6.49 \times 10^6$ IDV, $p < 0.0001$) and opt SARB scaffolds ($5.31 \times 10^5 \pm 1.41 \times 10^5$ IDV, $p = 0.0001$ and $2.20 \times 10^7 \pm 7.55 \times 10^6$ IDV, $p = 0.0011$) (Fig. 1A,B). Indeed, with targeted solubilization of both hydrophilic and lipophilic antigens, fold-increase in circulating graft-specific IgG titer for ASB-14 scaffolds was reduced compared to that observed for opt SARB scaffolds wherein solubilization of only hydrophilic antigens was promoted ($p < 0.05$) (Table 3 and Fig. 2A). Further, little to no local T-cells and small lymphoid follicles were observed with ASB-14 scaffolds (median cell-mediated immune response score of 1) (Table 2 and Fig. 2B,C). This minimal response against ASB-14 scaffolds was in contrast to the robust local cellular response against opt SARB scaffolds (median score of 5, $p < 0.0001$), characterized by numerous T-cells and large lymphoid follicles. Residual MHC I of opt SARB scaffolds was

not different than that of native BP ($p = 1.0000$); however, systemic and local adaptive responses to native BP were less than that to opt SARB scaffolds ($p < 0.05$ and $p = 0.0001$, respectively). Surprisingly, in spite of the aforementioned reduction in residual MHC I of ASB-14 scaffolds compared to native BP ($p = 0.0001$), neither systemic nor local adaptive responses against native BP were different than those towards ASB-14 scaffolds ($p > 0.05$ and $p = 0.6981$, respectively). No differences in either MHC I or α-gal levels between ASB-14 and SDS scaffolds ($1.28 \times 10^5 \pm 7.75 \times 10^4$ IDV, $p = 1.0000$ or $6.41 \times 10^6 \pm 8.50 \times 10^6$ IDV, $p = 0.9903$) is in agreement with the absence of difference in circulating antibody titers. However, SDS scaffolds were associated with greater local cellular response than ASB-14 scaffolds (median score of 2, $p = 0.0036$), characterized as moderate levels of lymphoid follicles and T-cells along the middle and ends of the implant. Although no differences in either MHC I or α-gal levels were determined between ASB-14 scaffolds and fixed BP ($1.57 \times 10^4 \pm 3.37 \times 10^4$ IDV, $p = 0.6466$ or $2.09 \times 10^6 \pm 2.86 \times 10^6$ IDV, $p = 0.9602$) and both implants were associated with little to no T-cells, fixed BP exhibited less systemic graft-specific response (i.e., temporal fold-increase in IgG titer) than any other scaffold ($p < 0.05$). However, ASB-14 scaffolds elicited less local cell-mediated immune response than fixed BP (median score of 2, $p = 0.0329$). Reduction of both hydrophilic and lipophilic antigens in ASB-14 BP scaffolds attenuated both systemic and local graft-specific rabbit adaptive immune responses compared to glutaraldehyde-fixation, decellularization, or hydrophilic solubilization alone.

3.2. Preservation of ECM architecture avoids recipient foreign body response

To discern the relationship between ECM architecture and recipient innate immune responses, BP scaffolds were characterized for pre-implantation ECM morphology, collagen alignment, and thermal stability. Following 42 d subpannicaular implantation in rabbits, collagen alignment and local innate immune responses (i.e., peri-implant macrophages and giant cells, and fibrous encapsulation) were assessed. On scanning electron microscopy, no changes in ECM morphology (i.e., gross wavy organization and fibril diameter) were observed for ASB-14 scaffolds compared to native BP on either the serous (Fig. 3A) or fibrous (Fig. S2) surfaces. Similarly, collagen alignment on polarized light microscopy was not different between ASB-14 scaffolds (30.52 ± 5.89% area) and native BP (33.27 ± 15.74% area; $p = 0.9871$) (Fig. 3A,B). Additionally, thermal stability of ASB-14 scaffolds (denaturation temperature 194.20 ± 1.19 °C) was not significantly different from that of native BP (denaturation temperature 194.97 ± 4.24 °C, $p = 0.9999$) (Fig. 3C). Maintenance of ECM architecture in ASB-14 scaffolds resulted in few, if any, graft-associated macrophages and thinner fibrous encapsulation (50.87 ± 66.69 μm) than all other groups ($p < 0.0001$ for fixed BP, SDS scaffold, and opt SARB scaffold; $p = 0.0136$ for native BP) (Fig. 2B,D). Although no changes in morphology, collagen alignment (28.73 ± 10.15% area; $p = 0.9237$), or thermal stability (denaturation temperature 197.41 ± 3.36 °C, $p = 0.9889$) of opt SARB scaffolds were detected compared to native BP, opt SARB scaffolds elicited the greatest macrophage response, present along the middle and cut ends of the biomaterial. However, fibrous encapsulation of opt SARB scaffolds (159.71 ± 119.67 μm) was not different than native BP (123.03 ± 88.73 μm, $p = 0.4858$). The wavy morphology of collagen bundles was less prominent in fixed BP than in native BP, particularly on the serous surface. Furthermore, presence of bright fibrils and dark void spaces, typically indicative of depth in

the z-dimension, was greatly reduced on fixed BP compared to native BP. Collagen organization in fixed BP was stratified, with some layers retaining collagen alignment and others having lost collagen alignment, resulting in an overall trend towards decreased alignment which failed to achieve statistical significance (20.20 ± 6.04% area, $p = 0.1641$) compared to native BP. Thermal stability of fixed BP was increased compared to that of native BP (denaturation temperature 220.90 ± 11.08 °C, $p = 0.0003$). This alteration of ECM architecture corresponded to moderate macrophage infiltration and greater fibrous capsule formation (209.06 ± 141.34 μm) than that of either ASB-14 scaffolds ($p < 0.0001$) or native BP ($p = 0.0016$). SDS scaffolds exhibited loss of wavy collagen morphology and thickening of collagen fibrils compared to native BP. Decreased collagen alignment (10.01 ± 6.63% area, $p = 0.0027$) and trend towards reduced thermal stability (denaturation temperature 180.81 ± 4.24 °C, $p = 0.0742$) in SDS scaffold implants compared to native BP resulted in moderate macrophage presence and substantial fibrous encapsulation (207.66 ± 166.62 μm) not different than fixed BP ($p = 1.0000$), but thicker than ASB-14 scaffolds ($p < 0.0001$) and native BP ($p = 0.0011$). As observed pre-implantation, collagen alignment of ASB-14 scaffolds (30.65 ± 6.92% area, $p = 0.9768$) and opt SARB scaffolds (31.21 ± 7.95% area, $p = 0.9898$) after 42 d implantation was not different compared to native BP (33.48 ± 4.90% area) (Fig. 4A,B). Fixed BP exhibited a trend towards decreased collagen alignment (20.10 ± 13.71% area, $p = 0.0994$), while SDS scaffolds possessed reduced alignment (9.68 ± 4.40% area, $p = 0006$). Maintenance of ECM architecture in ASB-14 BP scaffolds prevented rabbit foreign body response.

3.3. Removal of hydrophilic and lipophilic antigens reduces in vivo scaffold calcification

Chronic graft-specific immune responses and associated matrix damage have the potential to induce scaffold calcification. Calcification was heterogeneously distributed throughout all scaffolds; therefore, calcification was assessed qualitatively by magnification at first detection and quantitatively at sites of calcification as percent area of calcification and maximum particle size. Calcium deposits were most prominent in opt SARB scaffolds, evident at low magnifications (i.e., 40X) and widely distributed throughout the full scaffold thickness (Fig. 4A). All other scaffolds contained nonuniform distribution of sparse deposits which required higher magnifications (i.e., 100X and above) for visualization. Where calcium deposits were present, graft calcification was greatest in opt SARB scaffolds (4.65 ± 6.98% HPF, 1713.42 μm^2 maximum particle size) (Fig. 4A,C); ASB-14 scaffolds (0.30 ± 0.48% HPF, $p = 0.0007$; ≤96.41 μm^2), SDS scaffolds (0.28 ± 0.24% HPF, $p = 0.0007$; ≤38.66 μm^2), native BP (0.58 ± 0.58% HPF, $p = 0.0019$; ≤207.67 μm^2), and fixed BP (0.37 ± 0.29% HPF, $p = 0.0009$; ≤99.69 μm^2) were significantly less calcified. This binary response with opt SARB scaffolds eliciting greater recipient response than all other scaffolds was comparable to that observed for graft-specific IgG titers (Fig. 2A), suggesting that recipient adaptive immune response has a critical role in accelerated biomaterial calcification. Further, neither ECM architecture damage nor innate responses were reflective of ultimate scaffold calcification, suggesting that these factors are insufficient to mediate accelerated calcification in this model. Based on the reduced calcification of ASB-14 scaffolds compared to opt SARB scaffolds, removal of hydrophilic and lipophilic antigens is one method for reducing adaptive immune response-mediated calcification; however, based

on the infrequent calcification of other scaffolds, it may not be the only method of reducing implant calcification.

3.4. ASB-14 scaffolds are promising biomaterials for vascular regeneration

In addition to its greater adaptive and innate immune-compatibility, the ingrowth of marked spindle-shaped, non-immune cells into ASB-14 scaffolds—but not SDS scaffolds or fixed BP—suggested greater pro-regenerative potential (i.e., fostering recellularization, integration with surrounding tissue, and recapitulation of surrounding tissue features) of the biomaterial. Therefore, the ability of ASB-14 scaffolds to facilitate vascular regeneration was investigated in a porcine carotid patch angioplasty model. Excellent handling characteristics of ASB-14 and opt SARB scaffolds were more surgically favorable than fixed BP owing to greater flexibility and more rapid hemostasis. T-cells, B-cells, and lymphoid follicles were observed around the sutured ends of all patches (Fig. 5B). Fewer T-cells, B-cells, and lymphoid follicles were associated with ASB-14 scaffolds than opt SARB scaffolds, for which strong adaptive immune response was observed along the entire abluminal scaffold surface. T- and B-cell distribution around ASB-14 scaffolds was similar to that of fixed BP; however, fixed BP had fewer lymphoid follicles.

Twenty-eight days post-implantation, all animals receiving ASB-14 scaffolds achieved robust medial regeneration at the patch ends (81–121% native vessel thickness) (Fig. 5B,D). Specifically, ASB-14 scaffolds promoted complete endothelialization, development of a substantial medial smooth muscle cell layer, smooth muscle cell ingrowth into the implant, and pro-regenerative macrophage polarization (M2 > M1) at the patch middle (11.12 ± 11.35 M2:M1 ratio) and ends (16.59 ± 10.37 M2:M1 ratio) (Fig. 6). ASB-14 scaffold-patched arteries exhibited laminar flow with no evidence of either significant stenosis or aneurysmal dilation (Fig. 5A). Two animals receiving fixed BP achieved appropriate medial regeneration at the patch ends (77% and 96% native vessel thickness), but one animal exhibited substantial neomedial hyperplasia (350% native vessel thickness). Mid-patch, neomedial thickness with all fixed BP patches (2–42% native vessel thickness) was minimal (Fig. 5B,C). Endothelialization of fixed BP patches was discontinuous or absent. Although a thin smooth muscle cell layer was present with fixed BP, no smooth muscle cell ingrowth into the implant was observed. Additionally, pro-inflammatory macrophage polarization was observed at the middle (0.72 ± 0.54 M2:M1 ratio) and ends (0.82 ± 0.90 M2:M1 ratio) of fixed BP. Turbulent flow was observed with all fixed BP-patched arteries due to aneurysmal dilation in two animals and mild stenosis in the third. Additionally, one animal exhibited delamination and hemorrhagic dissection between the collagen fibers of the fixed BP patch. Taken together, these data support the ability of ASB-14 BP scaffold implants to foster vascular regeneration.

4. Discussion

This study demonstrates that stepwise solubilization-based removal of hydrophilic, followed by lipophilic antigens significantly reduces deleterious recipient graft-specific immune responses. Additionally, loss of ECM morphology, collagen alignment, and thermal stability following scaffold production may correlate with both onset of destructive innate immune

responses and absence of constructive regenerative recipient *in vivo* responses. Thus, significant reduction of hydrophilic and lipophilic antigens and maintenance of ECM architecture may permit rapid *in vivo* vascular regeneration. For the first time, to our knowledge, the role of residual antigenicity and ECM maintenance for a favorable recipient response is described (Fig. 7).

An ideal xenogeneic ECM scaffold should be recognized by recipient innate cells as self to avoid rejection and foreign body response. Chemical fixation alters ultrastructure, composition, and surface topology of tissue and promotes foreign body response-mediated encapsulation [5]. Indeed, fixed BP exhibited loss of collagen waviness, depth, and alignment with increased thermal stability indicative of structural alterations to ECM components from glutaraldehyde cross-linking. Although only a trend toward decreased collagen alignment of fixed BP was observed, the employed quantification method likely resulted in an overestimate of collagen alignment for fixed BP. Glutaraldehyde-fixation under pressure decreases native BP thickness by 79% (data not shown). Therefore, the resultant compression of collagen fibers in fixed BP effectively increases density of aligned collagen per unit area when calculated using post-fixation area. Fortunately, denaturation temperature is a direct quantification of ECM thermal stability. Difference in denaturation temperature of fixed BP compared to native BP provides additional evidence for disruption of ECM architecture in fixed scaffolds, since assessment of the bulk material is less susceptible to limitations of the collagen alignment analysis. This disruption of native ECM architecture facilitated innate immune cell recognition of fixed BP as non-self [5], stimulating a foreign body response characterized by large numbers of peri-scaffold giant cells (15–100 per slide) and significant fibrous encapsulation. Similarly, the significant compromise of ECM architecture in SDS-decellularized scaffolds likely resulted in up to 40 multinucleated giant cells per slide and fibrous capsule formation not significantly thinner than that of fixed BP. SDS-induced collagen fiber swelling [24,25] has been attributed to destabilization of the triple helical domain [26]. This perturbation from native collagen structure may have triggered innate cellular identification of SDS scaffolds as foreign material, leading to foreign body response similar to that observed with fixed BP. In contrast, maintenance of collagen waviness, collagen fibril diameter, collagen alignment, and thermal stability in ASB-14 scaffolds resulted in fewer than 5 peri-scaffold giant cells per slide and significantly less fibrotic encapsulation than any other group, implying that this biomaterial was recognized by the recipient innate immune system as native in origin. With recognition of ASB-14 scaffolds as a native ECM, innate immune cells may surveil it like normal tissue, rather than isolating it from the rest of the body. Collectively, these data indicate that preservation of native ECM architecture (i.e., morphology, collagen alignment, and thermal stability), achieved using stepwise solubilization of both hydrophilic and lipophilic antigens, is critical for avoiding innate immune system-mediated foreign body response towards the resultant ECM scaffold.

Decellularization and antigen removal methods intend to remove antigenic content from xenogeneic tissues to render the resultant ECM scaffold compatible with implantation in an immunocompetent recipient. Antigen removal using opt SARB alone predominantly removes hydrophilic BP antigens, leaving lipophilic antigen content largely unaffected [18]. Persistence of lipophilic antigens is supported by minimal removal of known membrane-

associated antigens MHC I and α-gal from opt SARB scaffolds. In this concordant xenotransplantation model, MHC I and other minor histocompatibility lipophilic xenoantigens were likely the mediators of the substantial number of local T-cell infiltrates and large lymphoid follicles associated with opt SARB scaffolds, suggesting that lipophilic antigen persistence is a critical determinant of *in vivo* adaptive immune response towards xenogeneic ECM scaffolds. Interestingly, large follicles were not observed with native BP tissue in spite of persistent hydrophilic and lipophilic antigens, including MHC I [18]. While only speculative without further experimentation, preservation of intact cells in native BP may have muted recipient response over the first 42 d post-implantation by shielding intracellular antigenic components. Over chronic time-frames, as antigenic contents of native BP tissue become increasingly accessible following cellular deterioration, it is possible the recipient response may continue to rise, ultimately reaching levels equal to or greater than that of opt SARB scaffolds. In fact, the moderate number of T-cells around native BP tissue supports occurrence of antigen recognition, which may be delayed compared to groups in which complete cell disruption had been achieved prior to implantation. Although SDS scaffolds achieved a 75% reduction in residual MHC I content and have previously been reported to have a 37% reduction in residual lipophilic minor histocompatibility antigens compared to opt SARB scaffolds [18], moderate T-cell infiltrate and lymphoid follicle presence persisted. The presence of 400% more residual hydrophilic minor histocompatibility antigens in SDS-decellularized scaffolds than opt SARB scaffolds [18] suggests that hydrophilic antigen persistence is also a critical determinant of *in vivo* adaptive immune response. Few, if any, T-cells or lymphoid follicles were observed around ASB-14 scaffolds or fixed BP, which agrees with absence of significant differences in residual MHC I levels between the two groups. However, decreased temporal graft-specific IgG response to fixed BP compared to ASB-14 scaffolds will require further investigation to understand long-term implications. While MHC I persistence in ASB-14 scaffolds was not different from SDS scaffolds, the reduction of minor histocompatibility hydrophilic and lipophilic antigens previously reported for ASB-14 scaffolds compared to SDS scaffolds [18] may explain the dramatic difference in local adaptive response between the two groups. Presence of spindle-shaped, non-inflammatory cells within ASB-14 scaffolds further suggests that macrophages and dendritic cells could also penetrate into the material; absence of macrophages and dendritic cells therefore further supports the low immunogenicity of ASB-14 scaffolds. Thus, these data suggest that adaptive immune responses can be substantially reduced with solubilization of both hydrophilic and lipophilic components of BP, while failure to address either hydrophilic or lipophilic fractions elicits local adaptive immune responses towards the ECM scaffold.

Tissue calcification leads to eventual destruction of chemically fixed biological tissue and failure of biological prostheses [27,28]. The mechanism for calcification of fixed BP has been attributed to damage from both chronic immune responses [27–29] and the fixation process [30–32]. Specifically, collagen damage in implanted xenografts may become a nucleus for calcium deposition [30,33]. Therefore, the severe adaptive immune responses elicited by residual lipophilic xenoantigens in opt SARB scaffolds agrees with substantial calcification of this implant. Moreover, this same collagen damage may also be responsible for the notable fibrous encapsulation of opt SARB scaffolds owing to deviation from native

collagen architecture and activation of innate immune response. *In vivo* calcification of fixed aortic leaflets due to residual lipids [34] underscores the need for removal of membrane lipids and associated lipophilic antigens. Although the subcutaneous leporine model utilized here permitted identification of the role of lipophilic antigens in BP calcification, it should be noted that substantial and differentiating calcification was not detected between fixed BP, SDS scaffolds, ASB-14 scaffolds, and native BP. As calcification of fixed BP has been reported in multiple studies [29–32], absence of notable calcification here merits comparison of ASB-14 scaffold to fixed BP in another model, such as the intramuscular model used by Wright et al. [35], to discern whether or not hydrophilic and lipophilic antigen removal is sufficient to avoid calcification. The ability of stepwise, solubilization-based antigen removal to reduce BP calcification—a precursor to graft degradation—is an encouraging indication of the effectiveness of this strategy to substantially decrease graft-specific recipient immune response and associated ECM damage.

To generate a functional biomaterial suitable for tissue engineering or regenerative medicine applications, a successful antigen removal process must also maintain cellular repopulation capacity. Recellularization confers multiple benefits onto the graft including protection from thrombotic events following endothelialization [14,36]; the ability to undergo ECM turnover, repair, adaptive remodeling, and growth [15,16]; and cell-mediated biological functionality —attributes fundamental to recapitulate native tissue functions. As expected, masking of cell binding domains by glutaraldehyde cross-links permitted little to no cellular repopulation of fixed BP. Similarly, the observed extremely low SDS scaffold repopulation is a well-documented phenomenon [37,38]. Although SDS toxicity [39] is a commonly thought to cause poor recellularization of scaffolds, altered ECM biochemistry or structure following SDS treatment has also been suggested as a possible cause [40]. The notable ingrowth of non-immune associated, spindle-shaped cells throughout the full thickness of ASB-14 scaffolds further supports the concept that preservation of ECM architecture is critical to support robust *in vivo* recipient recellularization. In sum, these data demonstrate that alteration of ECM architecture interferes with *in vivo* recellularization of BP ECM scaffolds.

Avoidance of destructive graft-specific innate and adaptive immune responses with maintenance of recipient cellular repopulation capacity motivated assessment of BP scaffolds generated using stepwise, solubilization-based antigen removal in a porcine model of vascular regeneration. Through avoidance of glutaraldehyde-fixation, ASB-14 scaffolds retained the excellent handling characteristics of native soft tissue, unlike the much stiffer fixed BP. Fixed BP patches required approximately 10 min and use of Surgicel to achieve hemostasis. As fixation is known to decrease the elastic modulus of BP [41], presumably via cross-links limiting extension of elastin and uncrimping of collagen, the inability of suture holes created in fixed BP to adequately contract around the suture facilitated greater suture-line bleeding. In contrast, hemostasis was achieved in under 2 min for ASB-14 scaffolds, indicating that maintained elasticity [18], owing to maintained elastin and collagen content, ECM organization, and tensile properties [18], may permit appropriate contraction of the biomaterial around the suture, minimizing suture-line bleeding. Additionally, ECM preservation in ASB-14 scaffolds facilitated formation of robust neointimal and neomedial layers (containing endothelial and smooth muscle cells, respectively) after only 28 d, which were absent from fixed BP. Further, the greater pro-regenerative M2 macrophage response to

ASB-14 scaffolds compared to that of fixed BP is in agreement with the classic pro-inflammatory M1 response associated with fixed tissues [5,42]. Finally, no aneurysm or stenosis was observed with ASB-14 scaffolds while aneurysmal dilation was seen with fixed BP. With encouraging results in rabbit, the moderate pig abluminal innate and adaptive immune response to ASB-14 scaffolds was somewhat unexpected. Although the abluminal response was greater towards ASB-14 scaffolds than fixed BP, this response was still less than that observed towards opt SARB scaffolds in which lipophilic antigens are known to persist. Further, localization of a recipient response to the suture region of all patches suggests that the response may in part be independent from the patch itself and instead attributed to the suture material. Assessment at later post-operative time points will be important to determine whether the abluminal response will be tolerated with completion of the ongoing luminal regenerative process. However, these data indicate that ASB-14 scaffold support robust porcine carotid regeneration.

For clinical translation, the reduction in tissue antigenicity necessary to achieve favorable *in vivo* outcomes remains to be determined. Lipophile solubilization during ASB-14 scaffold generation significantly reduced residual α-gal antigens compared to native BP. That α-gal levels between ASB-14 scaffolds and fixed BP were not significantly different has encouraging implications for ASB-14 scaffolds as current fixed BP materials have already been demonstrated to avoid α-gal mediated hyperacute rejection. Complete removal of all xenoantigens is unlikely to be an attainable goal, particularly while maintaining biomaterial structure-function properties and recellularization capacity of xenogeneic ECM. However, absolute absence of antigenicity may not be a necessary criterion for xenogeneic scaffold development. ECM turnover begins around 1 month post-implantation, with complete ECM turnover occurring approximately 6 months post-implantation [43]. ASB-14 scaffolds already exhibited vessel wall regeneration at 28 d post-implantation. Therefore, if tissue antigenicity can be sufficiently reduced for catastrophic immune-mediated destruction to be avoided for approximately 6 months, it is possible that the original xenogeneic scaffold will be entirely replaced with recipient ECM. After completion of ECM turnover, immune rejection concerns are likely to be alleviated. Compared to fixed BP, wherein physical blocking of xenoantigens from the recipient immune system recognition delays rejection, ASB-14 scaffolds may still possess accessible residual antigens which can stimulate *in vivo* immune response. However, the reduction of antigenicity in ASB-14 scaffolds may be acceptable since the mild immune response in both rabbit and pig models do not seem to have negatively impacted regenerative potential of the material. We have demonstrated that either residual antigen persistence or ECM component disruption is sufficient to stimulate fibrosis, which may compromise vessel patch patency and integrity. As ASB-14 scaffolds elicited the least innate and adaptive immune responses of unfixed scaffolds tested, they represent a potential alternative to currently employed fixed BP materials. Additional studies over longer time-frames will be necessary to evaluate the chronic *in vivo* immune-mediated response and completion of tissue regeneration achieved with ASB-14 scaffolds. Thus, translational promise of ASB-14 scaffolds from both immune and regenerative perspectives warrants further investigation.

5. Conclusions

Reduction of both hydrophilic and lipophilic antigens with stepwise, solubilization-based antigen removal is critical to decreased *in vivo* immune response towards BP implants. Promotion of lipophile solubilization following hydrophile solubilization substantially reduced local innate, local cell-mediated adaptive, local humoral-mediated adaptive, and systemic humoral immune responses beyond that achieved by hydrophile solubilization alone. Unlike SDS-decellularization and glutaraldehyde-fixation, ASB-14 preserved BP ECM architecture to overcome local foreign body response. Finally, non-immune cellular repopulation of ASB-14 scaffolds was robust throughout the full thickness of the biomaterial. In a proof-of-concept vessel patch pilot, constructive intimal and medial regeneration observed with BP scaffolds generated using ASB-14 was absent from fixed BP patches. Currently, glutaraldehyde-fixed BP has multiple clinical applications, including vascular repair, replacement heart valves, and general surgery, suggesting limitations of fixed tissues (i.e., fibrotic encapsulation, and incompatibility with cell repopulation and recipient-mediated positively remodeling) do not preclude use in patients. However, with the shift towards regenerative medicine and engineered tissues that better recapitulate native tissue function, limitations of fixed tissues will become more apparent. Biomaterials such as ASB-14-treated BP ECM scaffolds that avoid fibrous encapsulation and immune rejection while permitting cellular repopulation and remodeling represent a promising solution as the field advances. Evidenced by the presented work, stepwise, solubilization-based antigen removal is a promising strategy for xenogeneic scaffold generation in tissue engineering and regenerative medicine applications.

Supplementary Material

Refer to Web version on PubMed Central for supplementary material.

Acknowledgments

We thank James Cravotta and Dr. Boaz Arzi for rabbit surgery assistance; Dr. Kevin Grayson for pig surgery assistance; Dr. Clare E. Yellowley for facility access; Ms. Becky Horn for her polarized light microscopy assistance; and Ms. Alycia Cook for technical immunohistochemistry assistance. Funding support was received from the American Heart Association (11SDG4980023, LGG) and NIH (R01HL115205, LGG).

Appendix A. Supplementary data

Supplementary data related to this article can be found at http://dx.doi.org/10.1016/j.biomaterials.2016.03.024.

References

1. Li X, Guo Y, Ziegler K, Model L, Eghbalieh SDD, Brenes R, et al. Current usage and future directions for the bovine pericardial patch. Ann Vasc Surg. 2011; 25:561–568. [PubMed: 21276709]
2. Ho KJ, Nguyen LL, Menard MT. Intermediate-term outcome of carotid endarterectomy with bovine pericardial patch closure compared with Dacron patch and primary closure. J Vasc Surg. 2012; 55:708–714. [PubMed: 22226180]

3. Shinoka T, Breuer C, Tanel R, Zund G, Miura T, Ma P, et al. Tissue engineering heart valves: valve leaflet replacement study in a lamb model. Ann Thorac Surg. 1995; 60:S513–S516. [PubMed: 8604922]
4. Dohmen PM, Konertz W. Tissue-engineered heart valve scaffolds. Ann Thorac Cardiovasc Surg. 2009; 15:362–367. [PubMed: 20081743]
5. Badylak SF. Decellularized allogeneic and xenogeneic tissue as a bioscaffold for regenerative medicine: factors that influence the host response. Ann Biomed Eng. 2014; 42:1517–1527. [PubMed: 24402648]
6. Cascalho M, Platt JL. The immunological barrier to xenotransplantation. Immunity. 2001; 14:437–446. [PubMed: 11336689]
7. Yang YG, Sykes M. Xenotransplantation: current status and a perspective on the future. Nat Rev Immunol. 2007; 07:519–531.
8. McMorrow IM, Comrack CA, Sachs DH, DerSimonian H. Heterogeneity of human anti-pig antibodies cross-reactive with the Gal(alpha1,3)Galactose epitope. Transplantation. 1997; 64:501–510. [PubMed: 9275119]
9. Galili U. The [alpha]-gal epitope (Gal[alpha]1-3Gal[beta]1-4GlcNAc-R) in xenotransplantation. Biochimie. 2001; 83:557–563. [PubMed: 11522383]
10. Janeway, CA., Jr, Travers, P., Walport, M., Shlomchik, MJ. Immunobiology. fifth. Garland Science; New York and London: 2001.
11. Gilbert TW, Sellaro TL, Badylak SF. Decellularization of tissues and organs. Biomaterials. 2006; 27:3675–3683. [PubMed: 16519932]
12. Crapo PM, Gilbert TW, Badylak SF. An overview of tissue and whole organ decellularization processes. Biomaterials. 2011; 32:3233–3243. [PubMed: 21296410]
13. Goncalves A, Griffiths LG, Anthony R, Orton EC. Decellularization of bovine pericardium for tissue-engineering by targeted removal of xenoantigens. J Heart Valve Dis. 2005; 14:212–217. [PubMed: 15792182]
14. Xu H, Wan H, Zuo W, Sun W, Owens RT, Harper JR, et al. A porcine-derived acellular dermal scaffold that supports soft tissue regeneration: removal of terminal galactose-α-(1, 3)-galactose and retention of matrix structure. Tissue Eng Part A. 2009; 15:1807–1819. [PubMed: 19196142]
15. Park S, Kim WH, Choi SY, Kim YJ. Removal of alpha-Gal epitopes from porcine aortic valve and pericardium using recombinant human alpha galactosidase A. J Korean Med Sci. 2009; 24:1126–1131. [PubMed: 19949670]
16. Nam J, Choi S-Y, Sung S-C, Lim H-G, Park S-s, Kim S-H, et al. Changes of the structural and biomechanical properties of the bovine pericardium after the removal of α-Gal epitopes by decellularization and α-Galactosidase treatment. Korean J Thorac Cardiovasc Surg. 2012; 45:380–389. [PubMed: 23275920]
17. Wong ML, Leach JK, Athanasiou KA, Griffiths LG. The role of protein solubilization in antigen removal from xenogeneic tissue for heart valve tissue engineering. Biomaterials. 2011; 32:8129–8138. [PubMed: 21810537]
18. Wong ML, Wong JL, Athanasiou KA, Griffiths LG. Stepwise solubilization-based antigen removal for xenogeneic scaffold generation in tissue engineering. Acta Biomater. 2013; 9:6492–6501. [PubMed: 23321301]
19. Anderson JM, Rodriguez A, Chang DT. Foreign body reaction to biomaterials. Semin Immunol. 2008; 20:86–100. [PubMed: 18162407]
20. Orenstein SB, Saberski ER, Kreutzer DL, Novitsky YW. Comparative analysis of histopathologic effects of synthetic meshes based on material, weight, and pore size in mice. J Surg Res. 2012; 176:423–429. [PubMed: 22099590]
21. Junge K, Binnebösel M, von Trotha K, Rosch R, Klinge UP, Neumann U, et al. Mesh biocompatibility: effects of cellular inflammation and tissue remodelling. Langenbeck's Arch Surg. 2012; 397:255–270. [PubMed: 21455703]
22. Swartzlander MD, Blakney AK, Amer LD, Hankenson KD, Kyriakides TR, Bryant SJ. Immunomodulation by mesenchymal stem cells combats the foreign body response to cell-laden synthetic hydrogels. Biomaterials. 2015; 41:79–88. [PubMed: 25522967]

23. Samouillan V, Dandurand J, Lacabanne C, Thoma RJ, Adams A, Moore M. Comparison of chemical treatments on the chain dynamics and thermal stability of bovine pericardium collagen. J Biomed Mater Res Part A. 2003; 64A:330–338.
24. Henriquez M, Lissi E, Abuin E, Ciferri A. Assembly of amphiphilic compounds and rigid polymers. 1. Interaction of sodium dodecyl sulfate with collagen. Macromolecules. 1994; 27:6834–6840.
25. Krejčí J. Interaction of mixture of anionic surfactants with collagen. Int J Cosmet Sci. 2007; 29:121–129. [PubMed: 18489333]
26. Samouillan V, Dandurand-Lods J, Lamure A, Maurel E, Lacabanne C, Gerosa G, et al. Thermal analysis characterization of aortic tissues for cardiac valve bioprostheses. J Biomed Mater Res. 1999; 46:531–538. [PubMed: 10398014]
27. Human P, Zilla P. Characterization of the immune response to valve bioprostheses and its role in primary tissue failure. Ann Thorac Surg. 2001; 71:S385–S388. [PubMed: 11388230]
28. Manji RA, Zhu LF, Nijjar NK, Rayner DC, Korbutt GS, Churchill TA, et al. Glutaraldehyde-fixed bioprosthetic heart valve conduits calcify and fail from xenograft rejection. Circulation. 2006; 114:318–327. [PubMed: 16831988]
29. Kim MS, Jeong S, Lim HG, Kim YJ. Differences in xenoreactive immune response and patterns of calcification of porcine and bovine tissues in α-Gal knock-out and wild-type mouse implantation models. Eur J Cardiothorac Surg. 2015; 48:392–399. [PubMed: 25549993]
30. Levy RJ, Schoen FJ, Sherman FS, Nichols J, Hawley MA, Lund SA. Calcification of subcutaneously implanted type I collagen sponges. Effects of formaldehyde and glutaraldehyde pretreatments. Am J Pathol. 1986; 122:71–82. [PubMed: 3079959]
31. Golomb G, Schoen FJ, Smith MS, Linden J, Dixon M, Levy RJ. The role of glutaraldehyde-induced cross-links in calcification of bovine pericardium used in cardiac valve bioprostheses. Am J Pathol. 1987; 127:122–130. [PubMed: 3105321]
32. Kim KM, Herrera GA, Battarbee HD. Role of glutaraldehyde in calcification of porcine aortic valve fibroblasts. Am J Pathol. 1999; 154:843–852. [PubMed: 10079262]
33. Rodriguez KJ, Piechura LM, Porras AM, Masters KS. Manipulation of valve composition to elucidate the role of collagen in aortic valve calcification. BMC Cardiovasc Disord. 2014; 14:29. [PubMed: 24581344]
34. Levy RJ, Schoen FJ, Levy JT, Nelson AC, Howard SL, Oshry LJ. Biologic determinants of dystrophic calcification and osteocalcin deposition in glutaraldehyde-preserved porcine aortic valve leaflets implanted subcutaneously in rats. Am J Pathol. 1983; 113:143. [PubMed: 6605687]
35. Wright GA, Faught JM, Olin JM. Assessing anticalcification treatments in bioprosthetic tissue by using the New Zealand Rabbit intramuscular model. Comp Med. 2009; 59:266–271. [PubMed: 19619417]
36. Kasimir MT, Weigel G, Sharma J, Rieder E, Seebacher G, Wolner E, et al. The decellularized porcine heart valve matrix in tissue engineering: platelet adhesion and activation. Thromb Haemost. 2005; 94:562–567. [PubMed: 16268473]
37. Harrison RD, Gratzer PF. Effect of extraction protocols and epidermal growth factor on the cellular repopulation of decellularized anterior cruciate ligament allografts. J Biomed Mater Res Part A. 2005; 75A:841–854.
38. Reing JE, Brown BN, Daly KA, Freund JM, Gilbert TW, Hsiong SX, et al. The effects of processing methods upon mechanical and biologic properties of porcine dermal extracellular matrix scaffolds. Biomaterials. 2010; 31:8626–8633. [PubMed: 20728934]
39. Triglia D, Braa S, Yonan C, Naughton G. In vitro toxicity of various classes of test agents using the neutral red assay on a human three-dimensional physiologic skin model. In Vitro Cell Dev Biol Anim. 1991; 27:239–244.
40. Gratzer PF, Harrison RD, Woods T. Matrix alteration and not residual sodium dodecyl sulfate cytotoxicity affects the cellular repopulation of a decellularized matrix. Tissue Eng. 2006; 12:2975–2983. [PubMed: 17518665]
41. Hülsmann J, Grün K, El Amouri S, Barth M, Hornung K, Holzfuß C, et al. Transplantation material bovine pericardium: biomechanical and immunogenic characteristics after decellularization vs. glutaraldehyde-fixing. Xeno-transplantation. 2012; 19:286–297.

42. Brown BN, Valentin JE, Stewart-Akers AM, McCabe GP, Badylak SF. Macrophage phenotype and remodeling outcomes in response to biologic scaffolds with and without a cellular component. Biomaterials. 2009; 30:1482–1491. [PubMed: 19121538]

43. Bayrak A, Tyralla M, Ladhoff J, Schleicher M, Stock UA, Volk HD, et al. Human immune responses to porcine xenogeneic matrices and their extracellular matrix constituents in vitro. Biomaterials. 2010; 31:3793–3803. [PubMed: 20171732]

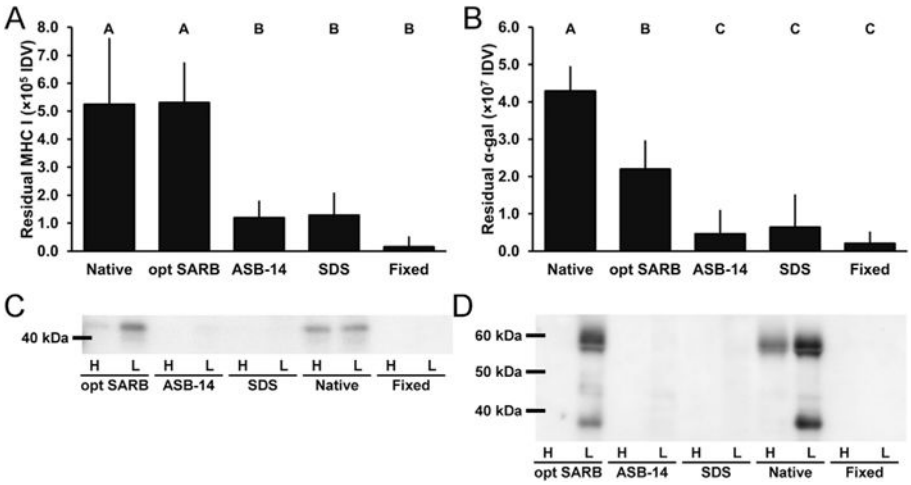

Fig. 1.

Known xenoantigen content of BP biomaterials. Residual MHC I (A) and α-gal (B) in BP biomaterials. Representative blots of extracted MHC I (C) and α-gal (D) in hydrophilic (denoted by "H") and lipophilic (denoted by "L") extracts of BP biomaterials. Results plotted as mean ± standard deviation ($n = 6$ per group). Groups not connected by same letter are significantly different ($p < 0.05$).

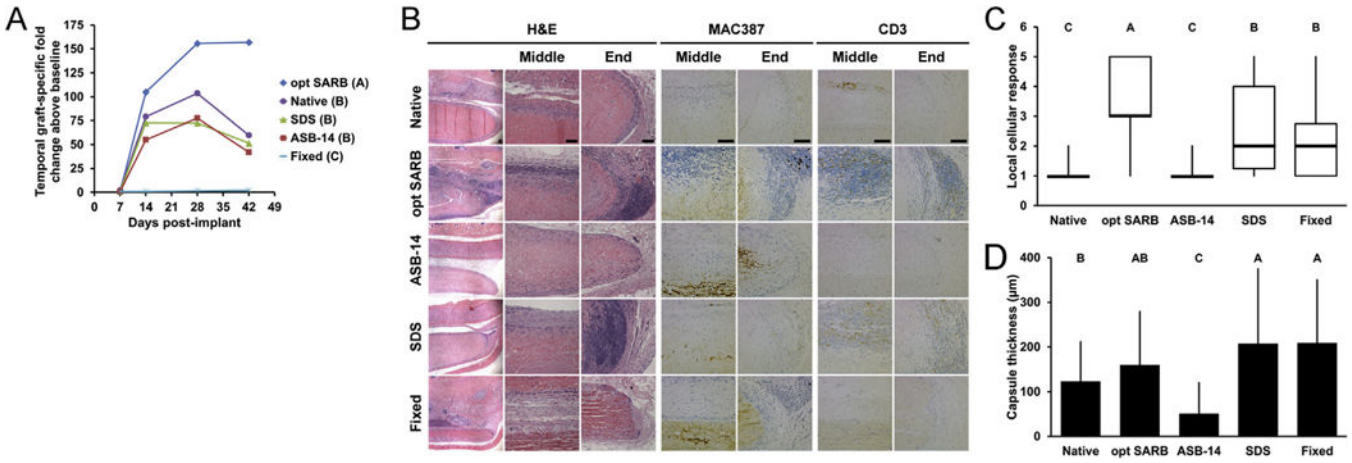

Fig. 2.

Systemic humoral, local innate and adaptive cellular, and local foreign body *in vivo* leporine responses to subpannicular BP implants. Temporal fold-increase in circulating graft-specific IgG titer post-implantation of BP implants (A). Representative images of BP implants at 42 d on H&E staining taken at low magnification (column 1), scaffold middle (column 2), and scaffold end (column 3). Representative images of MAC387 (macrophage, columns 4 and 5) and CD3 staining (T-cell, columns 6 and 7) staining taken at the middle and end of the scaffold at 42 d, respectively. Scale bar = 100 μm. Local cellular response as observed on H&E staining (C). Fibrous capsule thickness around BP implants at 42 d (D). Results plotted in (A) as mean ($n = 6$ per group and timepoint); (C) as mean ± standard deviation ($n = 6$ per group); and (D) as median (denoted by the thick line), inter-quartile range (25th–75th percentile), maximum (top whisker) and minimum (bottom whisker). Groups not connected by same letter are significantly different ($p < 0.05$).

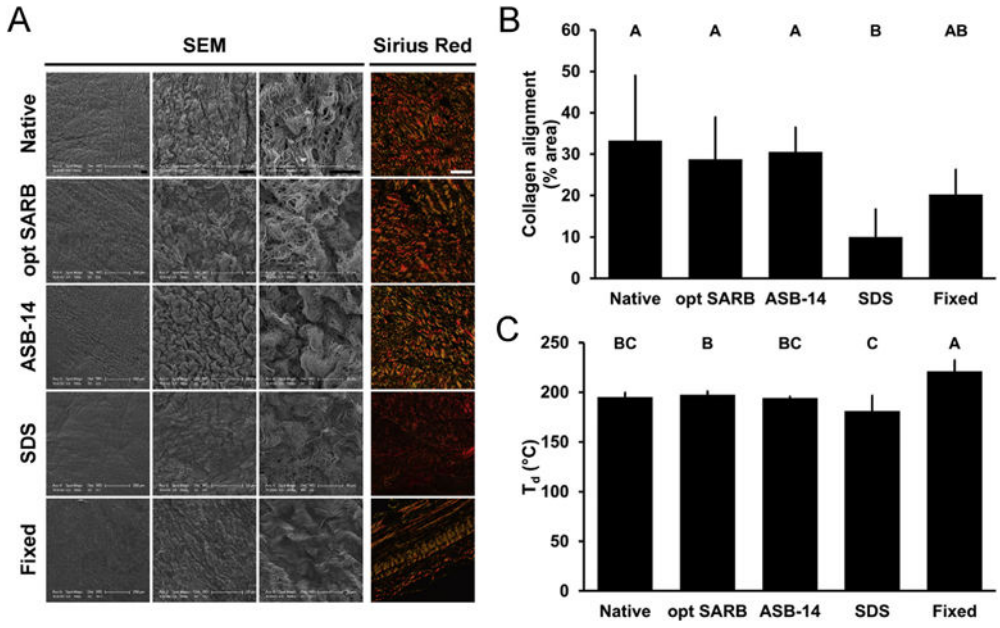

Fig. 3.

ECM architecture (morphology, collagen alignment, and thermal stability) of BP biomaterials. Representative images of BP biomaterials on scanning electron microscopy (serous side, columns 1–3) and picrosirius red staining under polarized light (column 4) (A). Scale bar = 100 μm unless otherwise stated. Collagen alignment of BP biomaterials observed on picrosirius red staining and expressed as percent area of field of view (B). Denaturation temperature (T_d) of BP biomaterials (C). Results plotted as mean ± standard deviation ($n = 6$ per group). Groups not connected by same letter are significantly different ($p < 0.05$). (For interpretation of the references to color in this figure legend, the reader is referred to the web version of this article.)

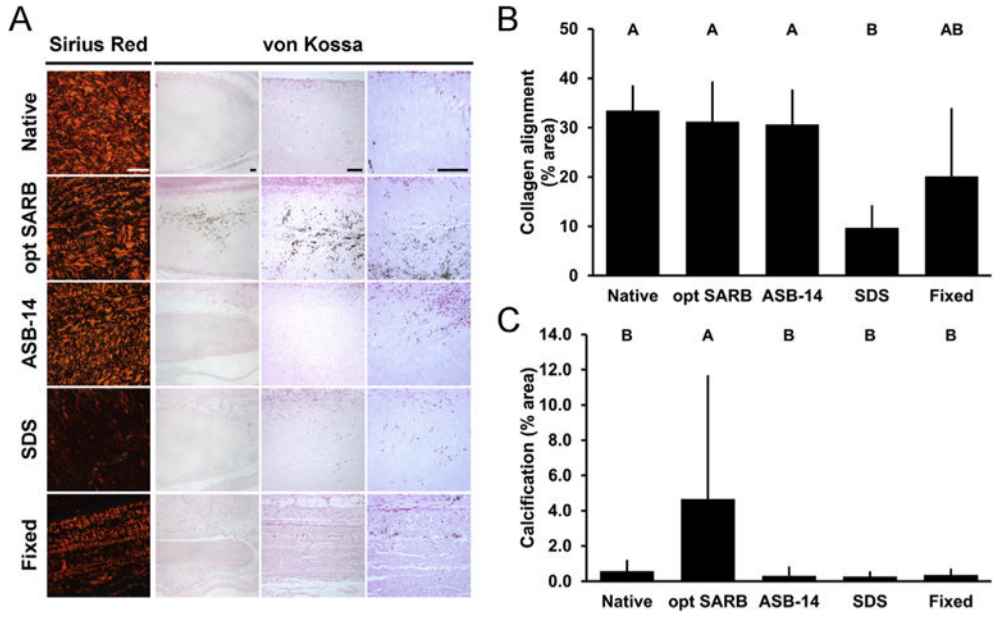

Fig. 4.

Collagen alignment and adaptive immune response-mediated *in vivo* calcification of leporine subpannicular BP implants. Representative images of 42 d BP implants on picrosirius red staining under polarized light (column 1) and von Kossa staining (Columns 2–4) (A). Scale bar = 100 μm. Collagen alignment of BP implants observed on picrosirius red staining and expressed as percent area of field of view (B). Adaptive immune response-mediated calcification of BP implants observed on von Kossa staining and expressed as percent area of field of view at sites of calcification (C). Results plotted as mean ± standard deviation ($n = 6$ per group). Groups not connected by same letter are significantly different ($p < 0.05$). (For interpretation of the references to color in this figure legend, the reader is referred to the web version of this article.)

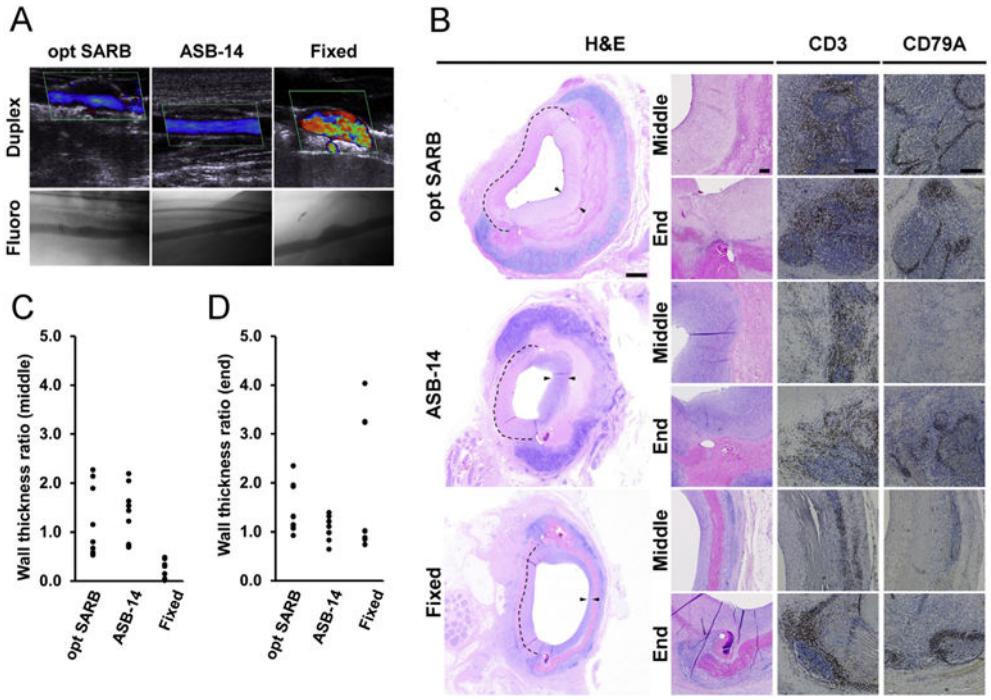

Fig. 5.

Flow profile, local innate and adaptive cellular, and pro-regenerative *in vivo* porcine responses to BP biomaterial vascular patches. Duplex ultrasound (top row) and fluoroscope (bottom row) images of BP biomaterial-patched porcine carotid artery at 28 d (A). Representative images of BP biomaterial vascular patches at 28 d on H&E staining taken at low magnification (column 1) and higher magnification at the patch middle and end (column 2) (B). Dotted line denotes original vessel wall and arrows denote neointima and neomedia at patch site. Representative images of CD3 (T-cell, column 3) and CD79A (B-cell, column 4) staining taken at the middle and end of the patch at 28 d. Scale bar = 1 mm (A, column 1) or 100 μm (A, columns 2–4). Ratio of combined intimal and medial wall thickness at patch middle (C) and end (D) to normal vessel thickness. Results plotted as individual observations (n = 9 per group).

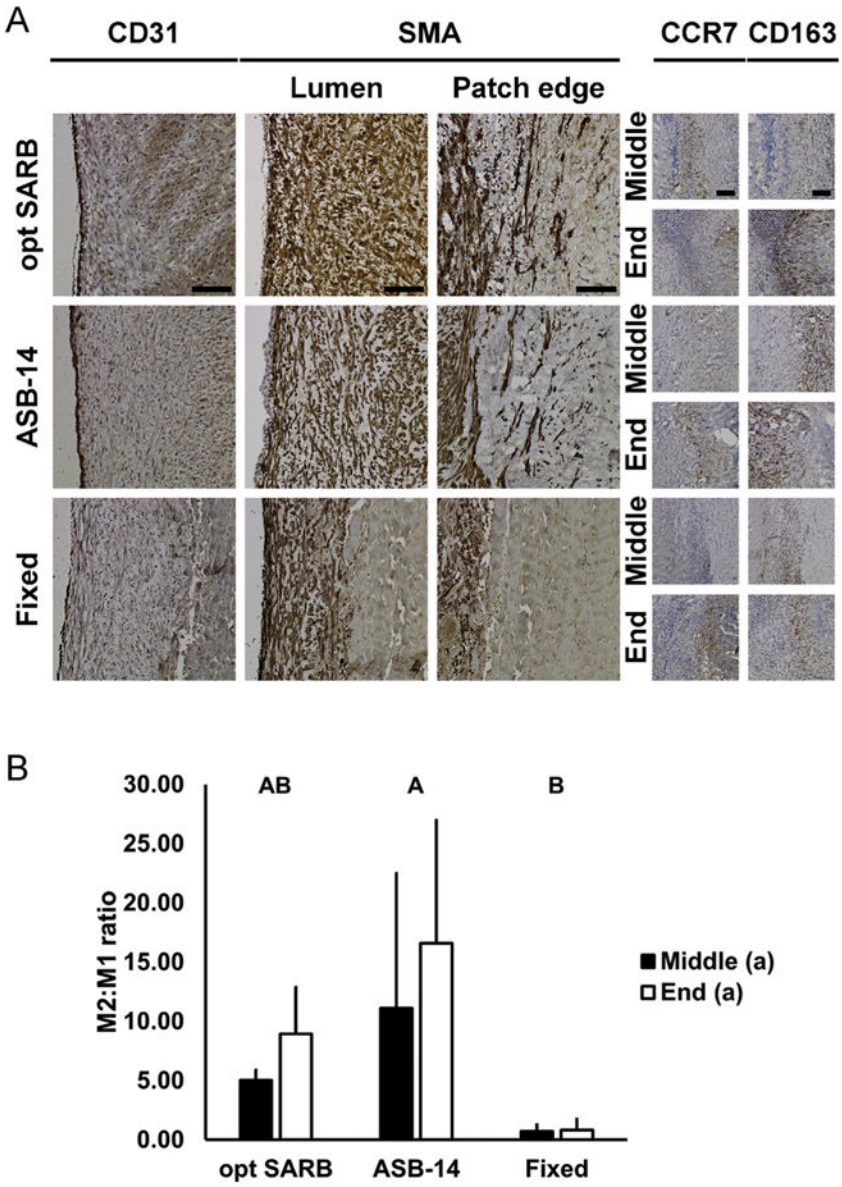

Fig. 6.

Pro-regenerative *in vivo* porcine responses to BP biomaterial vascular patches. Representative images of BP biomaterial vascular patches at 28 d on CD31 (endothelial cell, column 1) and SMA (smooth muscle cell, at lumen, column 2 and patch edge, column 3) staining (A). Representative colocalized images of BP biomaterial vascular patches at 28 d of CCR7 (M1 macrophage, column 4) and CD163 (M2 macrophage, columns 5) staining at patch middle (odd rows) and end (even rows). Scale bar = 100 μm. Ratio of M2 to M1 macrophages at patch middle and end (B). Results plotted as mean ± standard deviation ($n = 3$ per group and location). Groups not connected by same letter are significantly different ($p < 0.05$).

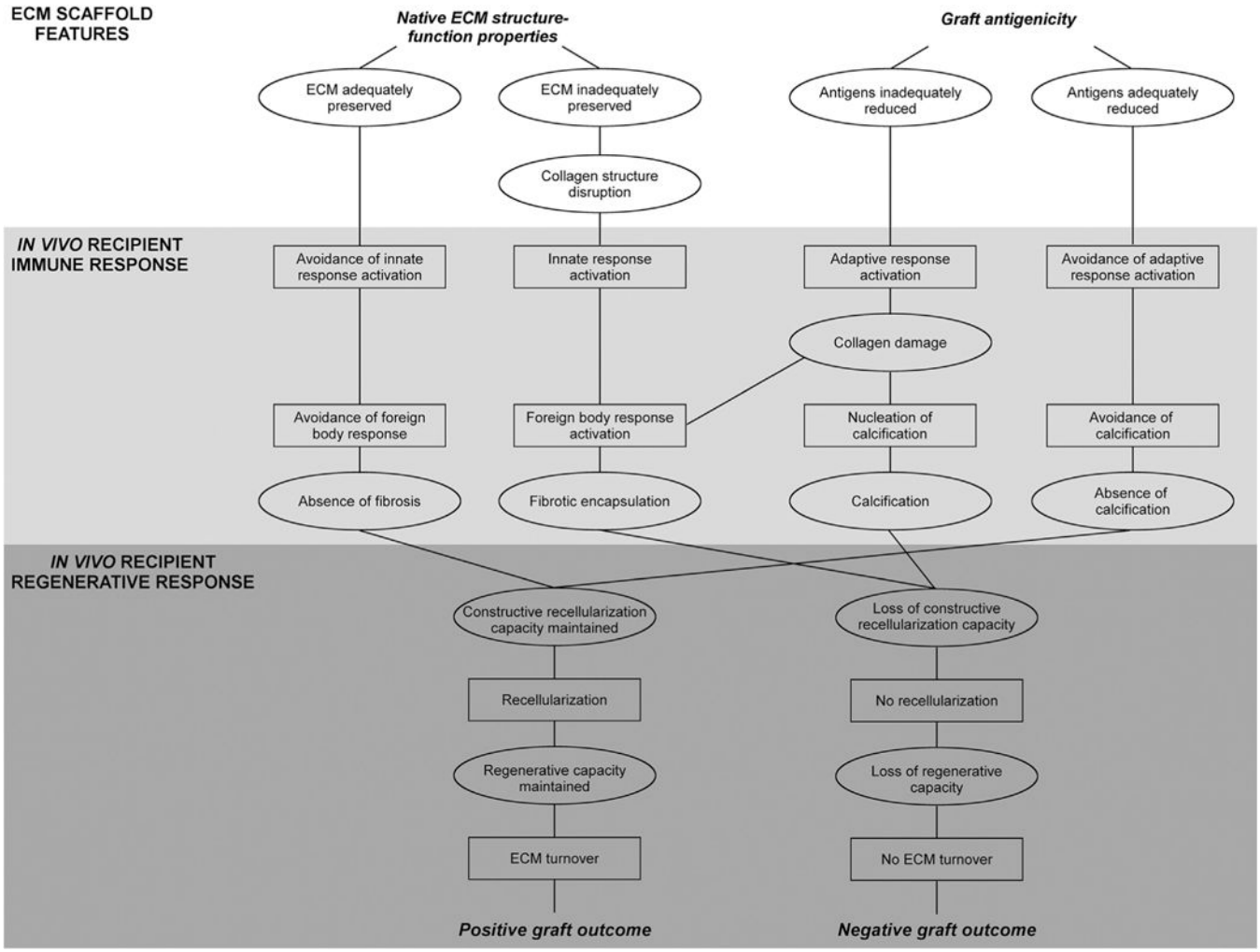

Fig. 7.

Proposed interplay of graft structure-function and antigenicity towards success of xenogeneic scaffold following implantation. In xenogeneic scaffold generation, antigenicity must be addressed to avoid negative graft-specific innate and adaptive immune responses, such as those observed with opt SARB scaffolds. However, scaffold structure-function properties must be maintained with processing to ensure the graft avoids negative remodeling responses, such as those observed with SDS scaffolds. By finding the balance between these properties, the resultant graft may facilitate positive regeneration. Scaffolds properties denoted by ellipses and *in vivo* recipient responses denoted by rectangles.

Table 1

Unfixed BP scaffold treatments.

Sample	Hydrophile solubilization	Lipophile solubilization
Native BP	–	–
opt SARB	opt SARB	–
ASB-14	opt SARB	1% (w/v) ASB-14 in opt SARB
SDS	0.1% (w/v) SDS in BARB	1% (w/v) SDS in BARB

Scaffolds were generated using hydrophile solubilization only (opt SARB), stepwise hydrophile and lipophile solubilization (ASB-14), or SDS-decellularization (SDS).

Table 2

Scoring scheme for leporine local cellular response to implanted BP scaffolds.

Score	Characteristics	
	Mononuclear inflammatory cell cuff	**Lymphoid structures**
0	None	None
1	Very thin, discontinuous	None
2	Thin, discontinuous or continuous	≤1 small aggregates
3	Thick, discontinuous or continuous	≤1 small aggregates
4	Thick, continuous	≤3 small follicles
5	Thick, continuous	>3 small or 1 large follicle(s)

Local cellular response scored by two blinded observers independently based on thickness and continuity of mononuclear inflammatory cell cuff, and quantity and size of lymphoid structures.

Table 3

Leporine systemic graft-specific adaptive response to implanted BP scaffolds.

Sample	Day 0	Day 7	Day 14	Day 28	Day 42	
Native BP	1.00 ± 0.00	2.13 ± 0.72	79.14 ± 61.61	103.65 ± 66.43	59.66 ± 25.01	B
opt SARB	1.00 ± 0.00	0.93 ± 0.09	104.82 ± 70.34	155.79 ± 95.64	156.91 ± 144.09	A
ASB-14	1.00 ± 0.00	0.89 ± 0.08	54.91 ± 45.84	77.66 ± 44.00	41.90 ± 22.93	B
SDS	1.00 ± 0.00	1.02 ± 0.19	72.64 ± 52.98	72.46 ± 27.64	51.41 ± 26.42	B
Fixed	1.00 ± 0.00	0.89 ± 0.06	0.90 ± 0.20	1.55 ± 0.96	2.02 ± 1.33	C
	b	b	a	a	a	

Temporal fold-change in circulating graft-specific IgG titer above 0 d. Results presented as mean ± standard deviation per scaffold type and timepoint (0–42 d) ($n = 6$ per group and timepoint). Groups not connected by same letter are significantly different ($p < 0.05$).